A&A 674, A213 (2023)
https://doi.org/10.1051/0004-6361/202346628

Astronomy & Astrophysics

A hidden population of white dwarfs with atmospheric carbon traces in the *Gaia* bifurcation

Maria Camisassa[1], Santiago Torres[1,2], Mark Hollands[3], Detlev Koester[4], Roberto Raddi[1,2], Leandro G. Althaus[5,6], and Alberto Rebassa-Mansergas[1,2]

[1] Departament de Física, Universitat Politècnica de Catalunya, c/Esteve Terrades 5, 08860 Castelldefels, Spain
e-mail: camisassam@gmail.com
[2] Institute for Space Studies of Catalonia, c/Gran Capità 2–4, Edif. Nexus 104, 08034 Barcelona, Spain
[3] Department of Physics and Astronomy, University of Sheffield, Sheffield S3 7RH, UK
[4] Institut für Theoretische Physik und Astrophysik, Christian-Albrechts-Universität, Kiel 24118, Germany
[5] Grupo de Evolución Estelar y Pulsaciones. Facultad de Ciencias Astronómicas y Geofísicas, Universidad Nacional de La Plata, Paseo del Bosque s/n, 1900 La Plata, Argentina
[6] Instituto de Astrofśica de La Plata, UNLP-CONICET, Paseo del Bosque s/n, 1900 La Plata, Argentina

Received 9 April 2023 / Accepted 3 May 2023

ABSTRACT

Context. The high-quality photometric and astrometric capabilities of the ESA *Gaia* space mission have revealed a bifurcation of the white dwarf sequence on the color magnitude diagram with two branches: A and B. While the A branch consists mostly of white dwarfs with hydrogen(H)-rich atmospheres, the B branch is not completely understood. Although it has been proposed that the B branch is populated mainly by helium (He)-rich white dwarfs, this branch overlaps with a ∼0.8 $M_{\odot}$ evolutionary track with a pure He envelope, which would imply an unexpected peak in the white dwarf mass distribution.
Aims. In cold He-rich white dwarfs, it is expected that the outer convective zone penetrates into deep carbon (C) -rich layers, leading to a slight C contamination in their surfaces at ∼10 000 K. In this paper we aim to study the *Gaia* bifurcation as the natural consequence of C dredge-up by convection in cold He-dominated white dwarfs.
Methods. Relying on accurate atmosphere models, we provide a new set of evolutionary models for He-rich white dwarfs, which employ different prescriptions for the C enrichment. On the basis of these models, we carried out a population synthesis study of the *Gaia* 100 pc white dwarf sample to constrain the models that best fit the bifurcation.
Results. Our study shows that He-rich white dwarf models with a slight C contamination below the optical detection limit can accurately reproduce the *Gaia* bifurcation. We refer to these stars as "stealth DQ" white dwarfs because they do not exhibit detectable C signatures in their optical spectra, but the presence of C in their atmosphere produces a continuum absorption favoring the emission in bluer wavelengths, thereby creating the B branch of the bifurcation. Furthermore, our study shows that the white dwarf mass distribution obtained when a stealth C contamination is taken into account presents a peak at ∼0.6 $M_{\odot}$, which is consistent with the mass distribution for H-rich white dwarfs and with the standard evolutionary channels for their formation.
Conclusions. We conclude that stealth DQ white dwarfs can account for the lower branch in the *Gaia* bifurcation. The C signatures of these stars could be detectable in ultraviolet (UV) spectra.

Key words. stars: evolution – white dwarfs – stars: atmospheres – stars: interiors

1. Introduction

White dwarfs are the most common end point of stellar evolution as they are the final destiny of more than 95% of the main sequence stars. These old compact objects, which are supported by electron-degeneracy pressure, undergo a slow cooling process that lasts for several gigayears (Gyr), turning these objects into reliable cosmochronometers allowing us to date stellar populations and main sequence companions; see, for instance, the reviews of Fontaine & Brassard (2008), Winget & Kepler (2008), Althaus et al. (2010), García-Berro & Oswalt (2016) and Córsico et al. (2019). Because of their unique characteristics, white dwarf stars are considered important objects for understanding the late stages of stellar evolution, as well as planetary systems and the structure and evolution of our Galaxy. Also, they can be used to infer the star formation rate, the initial mass function, the initial- to final-mass relation (IFMR), and the chemical evolution in the solar neighborhood (e.g., Rebassa-Mansergas et al. 2021; Raddi et al. 2022). Furthermore, the extreme densities that characterize the white dwarf interior make these stars promising laboratories with which to study stellar matter and energy sources under extreme conditions (e.g., Isern et al. 2022).

In recent decades, we have entered a golden era for the exploitation of white dwarf science. Surveys such as the Sloan Digital Sky Survey (SDSS, York et al. 2000), the RAdial Velocity Experiment (RAVE, Steinmetz et al. 2020a,b), the Panoramic Survey Telescope And Rapid Response System (PanSTARRS, Chambers et al. 2016) and others are providing the first large samples of moderate-resolution spectra and multi-band photometry for stars in our Galaxy (e.g., Kepler et al. 2021), and missions such as NASA Kepler and NASA Transiting Exoplanet Survey Satellite (TESS, Ricker et al. 2015) are providing measurements of photometric variations of these stars. In particular, the successive data releases by the ESA space mission *Gaia* constitute an unprecedented advance, providing multi-band

photometry, synthetic spectra, proper motions, and parallaxes for more than a billion sources (Gaia Collaboration 2018, 2021). Among these, Gentile Fusillo et al. (2021) identified nearly 360 000 high-confidence white dwarf candidates in the *Gaia* Data Release 3 (DR3), of which nearly 13 000 are within the 100 pc volume-limited sample (Jiménez-Esteban et al. 2018, 2023), leading the white dwarf research field into a new era.

The power of the *Gaia* space mission has revealed some unexpected features in the white dwarf cooling sequence on the color–magnitude diagram (CMD), identified as the A, B, and Q branches (see Gaia Collaboration 2018). The A branch is mainly populated by white dwarfs with H-rich atmospheres, that is DA spectral type, and overlaps with the evolutionary track of an approximately 0.6 $M_{\odot}$ white dwarf. On the other hand, the B branch constitutes a bifurcation from the A branch, has a significant fraction of He-rich white dwarfs, and lies on a ∼0.8 $M_{\odot}$ evolutionary track with a pure He envelope. Finally, the Q branch has a weaker concentration of white dwarfs and does not follow any evolutionary track or isochrone.

The origin of the Q branch has been extensively discussed in the literature, with the general consensus being that it arises from an energy released during white dwarf core crystallization (Tremblay et al. 2019; Cheng et al. 2019; Camisassa et al. 2021, 2022; Blouin et al. 2021; Caplan et al. 2021; Bauer et al. 2020; Fleury et al. 2022). In contrast, the origin of the AB bifurcation remains unclear, with no general consensus. El-Badry et al. (2018) attributed the existence of the bifurcation to a flattening in the IFMR, which leads to a secondary peak in the white dwarf mass distribution at approximately 0.8 $M_{\odot}$. Similarly, Kilic et al. (2018) also suggested the presence of this secondary peak, but these authors attributed it to the occurrence of stellar mergers. Alternatively, Ourique et al. (2020) proposed a different explanation for the origin of the *Gaia* bifurcation, suggesting that spectral evolution from a pure H to pure He envelope at an effective temperature ($T_{\rm eff}$) of ∼10 000 K in approximately 16% of DA white dwarfs may be an important contributing factor. Nevertheless, a recent study by Bergeron et al. (2019) found that assuming a pure He atmosphere for all non-DA white dwarfs leads to a low number of objects with masses of around ∼0.6 $M_{\odot}$ when $T_{\rm eff} < 11\,000$ K, which is inconsistent with the observed mass distribution at higher effective temperatures. These authors therefore suggested a He atmosphere with traces of H be considered instead (see also Serenelli et al. 2019). The additional electrons provided by traces of H in a He-rich white dwarf atmosphere cause a shift in the 0.6 $M_{\odot}$ evolutionary track, when $T_{\rm eff} <$ 11 000 K , thus creating the bifurcation. However, Bergeron et al. (2019) noticed that a significant fraction of He-rich white dwarfs should have H abundances that are sufficiently low that their photometric mass determinations at $8000\,{\rm K} \lesssim T_{\rm eff} \lesssim 10\,000\,{\rm K}$ are unaffected, and therefore a significant number of pure He white dwarfs with ∼0.6 $M_{\odot}$ would still be expected. These authors therefore suggested that another electron donor, such as C or metals, is required to fully explain the origin of the *Gaia* bifurcation.

In this paper, we aim to decipher whether or not the B branch of the CMD could be the result of the presence of C in the atmosphere of He-dominated white dwarfs. Theoretical models predict that He-dominated white dwarfs will dredge-up C as a result of convective mixing in the so-called PG1159-DO-DB-DQ spectral evolutionary channel (see Koester et al. 1982; Pelletier et al. 1986; Althaus et al. 2005; Dufour et al. 2005; Camisassa et al. 2017; Bédard et al. 2022). Unfortunately, the exact amount of C dredged-up in a He-rich white dwarf cannot be predicted by theoretical models. In particular, Bédard et al. (2022) followed the C enrichment from the beginning of the white dwarf cooling phase under different initial conditions and physical inputs, finding that the amount of C dredged-up by convection depends on the initial C surface abundance, the thickness of the He layer, the efficiency of extra mixing beyond the convective boundaries, and stellar mass. We find that the *Gaia* bifurcation can be explained by He-rich white dwarfs that experience a spectral evolution at $T_{\rm eff} \sim 12\,000$ K with a smooth C contamination just below the detection limits for optical spectroscopy. While this C contamination does not produce C lines in the optical spectra, it adds free electrons to the He envelope that produce a continuum opacity that shifts the 0.6 $M_{\odot}$ evolutionary track, causing the *Gaia* bifurcation. However, this C contamination has strong features in the UV spectra that could potentially be detectable.

This paper is organized as follows. In Sect. 2.1 we describe the white dwarf evolutionary models employed. In Sect. 2.2 we describe the C enrichment observed in white dwarfs determined in previous studies and the different prescriptions for the C enrichment adopted in this paper. In Sects. 2.3 and 2.4 we present details of the atmosphere models and the population synthesis code employed, respectively. In Sect. 3 we describe our results and, finally, in Sect. 4 we summarize the main findings of the study.

2. Methods

2.1. The white-dwarf cooling models

White dwarfs can be categorized based on the presence or absence of H in their atmospheres. It is thought that H is dominant in the atmospheres of nearly 80% of all white dwarfs (the so-called DA white dwarf class), and that the remaining 20% are depleted in H (the so-called nonDA white dwarf class) (Kepler et al. 2021; Jiménez-Esteban et al. 2023). The formation and evolution of H-rich white dwarfs is reasonably well understood and has been computed in several studies in the literature (for recent studies see e.g., Renedo et al. 2010; Althaus et al. 2015; Camisassa et al. 2016, 2019; Bédard et al. 2020; Salaris et al. 2022), and their pure H envelopes are the natural consequence of H floating up due to gravitational settling acting on an initial mixed H/He composition. Although a fraction of the H-rich white dwarfs could undergo spectral evolution due to convective dilution (Bédard et al. 2023), in this paper we assume that H-rich white dwarfs retain their H envelope throughout their evolution.

While DA white dwarfs have H-dominated atmospheres, most of the non-DA white dwarfs have atmospheres that are dominated by He. The evolution of white dwarfs with He-dominated atmospheres has been extensively studied over recent decades (Althaus et al. 2005; Camisassa et al. 2017; Salaris et al. 2022; Bédard et al. 2022). It is thought that He-rich white dwarfs are the descendants of the PG 1159 stars, which are hot stars with an envelope composed of He, C, and oxygen (O) in similar amounts. Initially, the C and O in the outer layers are supported by a weak radiative wind but as the white dwarf cools down, the wind weakens and the C and O rapidly sink into the stellar interior as a result of gravitational settling, leading to a pure-He atmosphere. This pure-He-envelope white dwarf should present He absorption lines, being classified first as a DO (He II lines) and later on as a DB (He I lines). As the white dwarf cools down, a convection zone gradually develops within the He envelope, growing inward and ultimately reaching the previously settled C, which, depending on the He layer thickness, is carried back to the surface. This spectral evolution transforms the

pure He DB white dwarf into a DQ white dwarf, that is, a He-dominated atmosphere white dwarf containing traces of C.

In this paper, we employ the H-rich evolutionary models of Camisassa et al. (2016), which are the result of the full evolution of progenitor stars starting at the zero age main sequence and evolved through the central H and He burning, the asymptotic giant branch (AGB), and the post-AGB phases, as calculated in Miller Bertolami (2016). These models commence the white dwarf phase with a H-dominated atmosphere with small amounts of He, C, and O. However, due to gravitational settling, the heavier elements sink rapidly, causing the outer envelope of the white dwarf to become entirely composed of H.

For He-dominated white dwarfs (nonDA), we employed the evolutionary models calculated in Camisassa et al. (2017), which are the result of the full progenitor evolution through the born-again scenario (see Camisassa et al. 2017; Miller Bertolami & Althaus 2006, for details). These models follow the complete white dwarf evolution from the PG 1159 stage at the beginning of the white dwarf cooling sequence, all the way to very low luminosities, keeping track of the gravitational settling of the C left in the envelope by the born-again evolution, and its later convective dredge-up. Although these models do not predict the correct amount of C dredge-up to the surface, we amended this issue by employing different artificial parametrizations for the C abundance that match the observed C sequence (see Sect. 2.2). It is worth noting that the cooling times considered in these models are expected to be realistic, as they take into account all relevant sources and sinks of energy and use accurate initial chemical profiles derived from the full progenitor evolution.

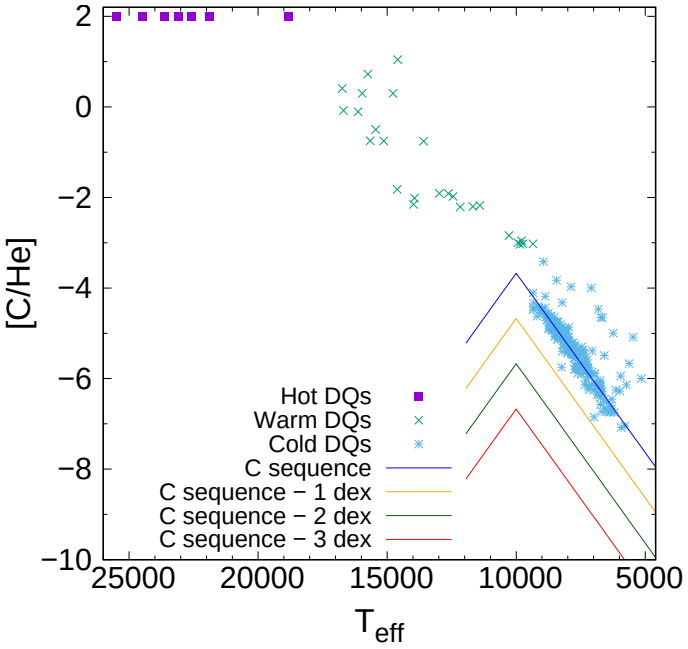

Fig. 1. Carbon to helium surface abundance ratio ([C/He]) vs. effective temperature for the hot DQs (purple squares), warm DQs (green crosses), and cold DQs (light-blue asterisks) taken from Koester & Kepler (2019). We note that, for the hot DQs, [C/He] has been fixed as the typical lower limit. The blue line is our parametrization for the observed [C/He] trend (the C sequence), and the orange, green, and red lines are the C sequence −1, −2, and −3 dex, respectively (see text for details).

2.2. The carbon enrichment

As mentioned above, theoretical models suggest that He-rich white dwarfs experience spectral evolution when their outer convective zone penetrates into C-rich layers, transforming them into DQ white dwarfs. The surface C abundance should grow until the convective zone reaches its maximum depth, and starts to decrease gradually as a result of C recombination at the bottom of the convective zone, which makes C sink into the interior (Pelletier et al. 1986). Bédard et al. (2022) recently investigated the evolution of the surface C abundance under different assumptions and found that it is strongly influenced by the initial conditions and physical inputs considered in the modeling. First, a higher C abundance at the beginning of the white dwarf phase and a thinner He envelope would be reflected in a larger amount of C dredged-up by convection (see Figs. 9 and 10 of Bédard et al. 2022, respectively). In addition, the stellar mass and the efficiency of extra mixing beyond the convective boundaries play a key role in determining the C-enrichment sequence. Thus, while theoretical models predict convective C dredge-up and a subsequent decrease in C abundance due to its recombination, they cannot accurately determine the exact C abundance in cold nonDA white dwarfs. Therefore, observational data are necessary to provide insights into this matter.

The white dwarfs showing C lines or molecular C in their spectra can be classified into three groups with markedly different characteristics: hot, warm, and cold DQs. Figure 1 shows the logarithm of the ratio between the numerical abundances of C and He ([C/He]) versus effective temperature determinations from Koester & Kepler (2019) for the hot, warm, and cold DQs using purple squares, green crosses, and light-blue asterisks, respectively. It should be noted that [C/He] for hot DQs has been set to the typical lower limit. The hot and warm DQs have considerably higher velocities, masses, and C abundances than cold DQs. Therefore, it is very unlikely that the hot and warm DQs are the predecessors of cold DQs, and their origin has been attributed to stellar mergers (Dunlap & Clemens 2015; Kawka et al. 2023). Furthermore, theoretical models of convective C dredge-up in He-rich envelopes fail to reproduce C enrichment in hot and warm DQs, but they can account for the C abundances at $T_{\rm eff} \lesssim 12\,000$ K observed in cold DQs. Based on the above information, cold DQs are thought to be the descendants of He-rich DB white dwarfs that became C enriched when the outer convective zone penetrated into C rich layers.

Koester et al. (2020) estimated the total He mass in the envelope of cold DQs by integrating the envelope equations from the outside using observed surface abundances as a starting point. These authors found that the total He mass fraction, q(He), in the envelope of cold DQs is independent of their effective temperature. These authors also found that the convection zone is marginally deeper for the colder DQs. These results support the idea that the cold DQ white dwarfs constitute an evolutionary path of white dwarfs with similar characteristics, and that the gradual decrease in [C/He] is caused by the C recombination at the base of the He envelope. Even when including overshooting in their calculations, these authors obtained q(He) ~ -3, which is nearly one order of magnitude lower than predicted from stellar evolution (Miller Bertolami & Althaus 2006; Althaus et al. 2009). Therefore, we can speculate that white dwarfs may have a wider range of He masses than expected – possibly depending on the number of thermal pulses experienced in the progenitor evolution – and that the cool DQs originate from the white dwarfs with the thinnest He envelopes.

In this paper, we present He-rich white dwarf models (nonDA) that follow the PG1159-DO-DB-DQ evolutionary

connection, and experience C dredge-up as a result of convective dilution. In order to mimic the C enrichment sequence, we consider that these white dwarfs have a pure He envelope if $T_{\rm eff} > 12\,000$ K and a He envelope containing traces of C if $T_{\rm eff} < 12\,000$ K. We considered four different prescriptions for the [C/He] ratio when $T_{\rm eff} < 12\,000$ K. The first set of white dwarf models follows the observed C enrichment sequence in terms of the effective temperature (which we refer to as the "C sequence" hereafter). The C sequence follows a linear least-squares fit to the observed C sequence reported in Table 1 of Koester et al. (2020) when $T_{\rm eff} < 10\,000$ K. To parameterize the range $12\,000$ K $> T_{\rm eff} > 10\,000$ K, we reflected this linear fit from $T_{\rm eff} = 10\,000$ K, mimicking the rise in the C abundance due to the deepening of the outer convective zone. The run of [C/He] in terms of the effective temperature of the C sequence is depicted using a blue line in Fig. 1. The cool region ($T_{\rm eff} \lesssim 10\,000$ K) of the C sequence is approximately on the optical detection limit of C for a signal-to-noise ratio $S/N = 20$ according to the DQ model atmospheres of Blouin et al. (2019). The [C/He] ratio in terms of the effective temperature in the second, third, and fourth sets of white dwarf models is that of the C sequence, but shifted −1 dex , −2 dex, and −3 dex, respectively (orange, green, and red lines in Fig. 1). Although C would still be present in their atmospheres, these three sets of models would not show C features in their optical spectra, and would therefore be classified as DC (see Sect. 2.3). These models account for the white dwarfs with thicker He envelopes than the one obtained for the C sequence in Koester et al. (2020). When [C/He] reaches values lower than −10.41, we consider a pure He atmosphere. It is important to remark that we only implemented this C-enrichment prescription in the atmosphere models, but the white dwarf structure and evolution is that of Camisassa et al. (2017), where the C enrichment as a result of convective dredge-up is considered, but does not follow the enrichment that we desire to simulate.

2.3. The atmosphere models

We calculated a grid of model atmospheres from Koester (2010) and Koester & Kepler (2019) for different $T_{\rm eff}$, surface gravity, and chemical composition, and then integrated their fluxes in different passbands. In particular, we employed three sets of atmosphere models: one with a pure H composition, one with a pure He composition, and one with a mixed He/C composition. The He/C ratio in the mixed composition models can vary according the C-enrichment prescription described in Sect. 2.2.

In Fig. 2 we show the synthetic spectra for atmosphere models with $\log g = 8.0$ and $T_{\rm eff} = 8000$ K and different chemical compositions: [C/He] = −5.2 (C sequence), [C/He] = −6.2 (C sequence −1 dex), [C/He] = −7.2 (C sequence −2 dex), [C/He] = −8.2 (C sequence −3 dex), and pure He. The spectrum of the C sequence atmosphere has strong C features, both in the optical and UV wavelengths. On the contrary, the atmosphere models with lower [C/He] and the pure He model do not show spectral lines or molecular Swan bands in the optical, and their spectra therefore resemble continuum; objects with such atmospheres would therefore be classified DC if observed at these wavelengths. Regarding the UV spectra, the C-contaminated models show C I absorption lines at 1931 Å and 2479 Å, which are more noticeable when the C abundance is higher. We decided to refer to the cold white dwarfs ($T_{\rm eff} \lesssim 12\,000$ K) with a trace [C/He] abundance of below the C sequence as "stealth DQs"; these objects do not present C features in the optical spectra but do show them in the UV wavelengths.

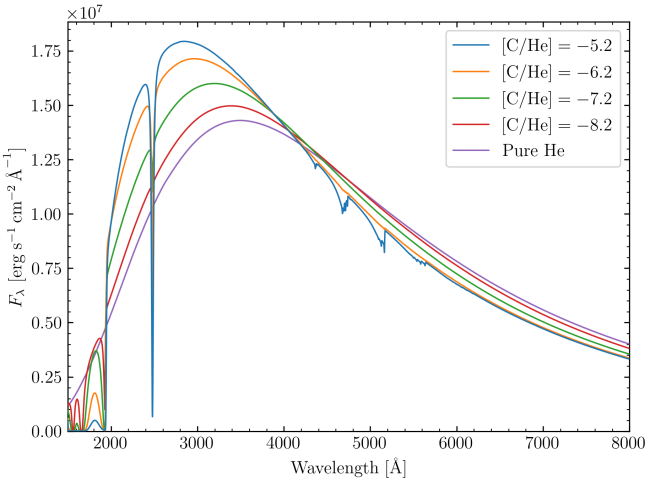

Fig. 2. Synthetic spectra for atmosphere models with $\log g = 8.0$ and $T_{\rm eff} = 8000$ K. The pure He model is shown with a purple line. The other models assume [C/He] = −5.2 (blue line, the C sequence), [C/He] = −6.2 (orange line, the C sequence −1 dex), [C/He] = −7.2 (green line, the C sequence −2 dex), and [C/He] = −8.2 (red line, the C sequence −3 dex).

Although the stealth DQ white dwarfs would appear as DC when observed in the optical wavelengths, their optical fluxes still differ from a pure-He model, because their continuum emission is shifted to bluer wavelengths (see Fig. 2). The more abundant the trace C is, the bluer the white dwarf becomes. The origin of this shift is the increase in the He^- free–free absorption, which is markedly altered by the presence of C. At low effective temperatures, only a tiny fraction of He becomes ionized to provide free electrons, and so only a very small amount of He^- can form in a pure-He atmosphere. Because C has a much lower ionization potential than He, only trace amounts of C are required for it to become the primary electron donor, allowing for a higher number of He^- ions to form, which in turn increases the He^- opacity, causing the shift to bluer wavelengths.

2.4. The population synthesis code

We performed a population synthesis analysis of the white dwarf thin-disk population within 100 pc – previously classified in Torres et al. (2019) – in order to provide insight into the C enrichment sequence. We employed a Monte Carlo population synthesis code widely used in the study of the single (e.g., García-Berro et al. 1999; Torres et al. 2005, 2021; Torres & García-Berro 2016; Jiménez-Esteban et al. 2018) and binary (e.g., Camacho et al. 2014; Cojocaru et al. 2017; Canals et al. 2018; Torres et al. 2022) white dwarf populations, as well as in studies of open and globular clusters (e.g., García-Berro et al. 2010; Torres et al. 2015) and the Galactic bulge (Torres et al. 2018). A detailed description of the code can be found in these latter publications. Therefore, in this paper, we provide a brief overview of the key inputs to the code.

Synthetic main sequence stars are generated with masses randomly following an initial mass function with a Salpeter distribution, considering $\alpha = -2.35$ and a minimum mass of $0.4\,M_\odot$. We assume a constant star formation rate, with a maximum age of 10.5 Gyr. Alternative prescriptions for the star formation rate and the total age will not affect the robustness of our results, because we are interested in analyzing only the *Gaia* bifurcation. Once each main sequence star is generated,

we employ the pre-white dwarf age of the Basti database (Hidalgo et al. 2018) to see which stars had time to become white dwarfs. Using an IFMR, we can then obtain the white dwarf masses and cooling times. We considered two different IFMRs: Catalán et al. (2008) and El-Badry et al. (2018). The initial metallicity of all the synthetic stars in this study was fixed to $Z = 0.02$, because we do not expect the metallicity distribution to alter our results. After obtaining the white dwarf cooling time and mass, we employed the white dwarf evolutionary models of the La Plata group described in Sect. 2.1 to obtain its physical properties, such as luminosity, effective temperature, surface gravity, and radius. We randomly assign an envelope composition to each white dwarf, either H-dominated (DA) or He-dominated (nonDA). We considered four different proportions of DA to nonDA white dwarfs: 100:0, 80:20, 75:25, and 70:30, respectively. For DA white dwarfs, we assumed that they preserve a pure H envelope throughout their evolution. For nonDA white dwarfs, we consider a pure He envelope if $T_{\rm eff} > 12\,000$ K, and if $T_{\rm eff} < 12\,000$ K, we consider that either the white dwarf retains this pure He envelope or that it undergoes C enrichment. In the simulations where we consider C enrichment in the synthetic populations, we assume the C sequence −0 dex, −1 dex, or −2 dex. We also simulated the possibility that each white dwarf may follow a different C enrichment sequence by randomly assigning a number in the range from 0 to 3 with a uniform distribution and subtract this number from the [C/He] expected for the C sequence. We named this type of C enrichment "C random [0:3]", because it assumes that each individual white dwarf can undergo a different C-enrichment sequence. A similar C-enrichment sequence was also considered, named "C random [0:2]", which assumes a random C distribution, but this time the random number assigned can vary in the range from 0 to 2, making this synthetic population more C enriched. Finally, in order to compare with the observational sample, we employ the atmosphere models described in Sect. 2.3 to convert the quantities from our evolutionary models into magnitudes in the *Gaia* passbands, and we added observational uncertainties by introducing photometric and astrometric errors in concordance with *Gaia* performance[1].

A total of 22 synthetic white dwarf populations models were generated, varying the proportion of DA to nonDA, the nonDA envelope composition, and the IFMR. The main characteristics of these synthetic population models are described in Table 1.

Table 1. Main characteristics of each of our synthetic population models and the χ^2 values obtained from the comparison with the observed sample (see text for details).

Ratio DA nonDA	NonDA composition	IFMR	χ^2
100% DA	–	(1)	4.046
100% DA	–	(2)	8.530
80% DA, 20% nonDA	Pure He	(1)	3.816
80% DA, 20% nonDA	Pure He	(2)	7.863
80% DA, 20% nonDA	C sequence	(1)	2.972
80% DA, 20% nonDA	C sequence	(2)	6.447
80% DA, 20% nonDA	C sequence −1 dex	(1)	3.191
80% DA, 20% nonDA	C sequence −1 dex	(2)	6.801
80% DA, 20% nonDA	C sequence −2 dex	(2)	7.019
80% DA, 20% nonDA	C random [0:2]	(1)	3.042
80% DA, 20% nonDA	C random [0:3]	(1)	3.147
80% DA, 20% nonDA	C random [0:3]	(2)	6.693
75% DA, 25% nonDA	C sequence	(1)	3.116
75% DA, 25% nonDA	C sequence −1 dex	(1)	3.228
75% DA, 25% nonDA	C random [0:2]	(1)	3.153
70% DA, 30% nonDA	Pure He	(1)	4.097
70% DA, 30% nonDA	C sequence	(1)	3.154
70% DA, 30% nonDA	C sequence −1 dex	(1)	3.380
70% DA, 30% nonDA	C sequence −2 dex	(1)	3.735
70% DA, 30% nonDA	C random [0:2]	(1)	3.079
70% DA, 30% nonDA	C random [0:3]	(1)	3.126

References. (1) Catalán et al. (2008); (2) El-Badry et al. (2018).

3. Results

3.1. Effects of carbon enrichment on the Gaia CMD

Figure 3 displays the effect of the atmospheric composition on the white dwarf evolutionary models in the *Gaia* CMD. The gray dots are the *Gaia* DR3 observations of the white dwarfs within 100 pc, whereas the solid lines depict 0.58 $M_\odot$ evolutionary models under different atmospheric compositions. In this plot, we can see the *Gaia* bifurcation into branches A and B, starting at $G \sim 12$ and $G_{\rm BP} - G_{\rm RP} \sim 0$. We note that the model with a pure H envelope (black solid line) overlaps with the upper branch of the *Gaia* bifurcation. Additionally, we can see that, although a 0.58 $M_\odot$ pure-He model (purple line) can somewhat better reproduce the lower branch of the bifurcation than a 0.58 $M_\odot$ pure-H model, a higher mass (∼0.8 $M_\odot$) pure-He model would overlap with this branch. The blue, orange, green, and red lines display 0.58 $M_\odot$ cooling sequences that mimic the C dredge-up enrichment. These cooling sequences have a pure He atmosphere if $T_{\rm eff} > 12\,000$ K and a He atmosphere with traces of C if $T_{\rm eff} < 12\,000$ K. The C-enrichment sequence in each of these evolutionary models is described in Sect. 2.2. By inspecting this figure, we can see that the 0.58 $M_\odot$ models with C enrichment overlap the lower branch of the *Gaia* bifurcation, and that the pure H and pure He models do not. As expected, the lower the trace C abundance, the closer to the pure He model the evolutionary sequence appears. We can conclude that the *Gaia* bifurcation occurs at $T_{\rm eff} \sim 10\,000$ K, which is roughly where we expect the surface C abundance to reach its maximum value, regardless of the input conditions on the modeling (see Figs. 7–12 in Bédard et al. 2022).

It is important to recall that, a C trace abundance of just 1 dex below the observed C sequence would be undetectable in optical observations. Therefore, trace C dredge-up by convection in a He-dominated atmosphere can be the source of opacity that causes the *Gaia* bifurcation. This conjecture is supported by the fact that most of the white dwarfs in the lower branch of the *Gaia* bifurcation are nonDA white dwarfs (65% according to Jiménez-Esteban et al. 2023).

3.2. Population synthesis analysis

In order to test the plausibility of the C enrichment in He-dominated white dwarfs being the mechanism responsible for creating the lower branch of the *Gaia* bifurcation, we performed a population synthesis analysis of the 100 pc thin-disk white dwarf population. The stellar density in the CMD (Hess diagram) of the observed sample is shown in Fig. 4. The *Gaia* bifurcation can easily be seen in this stellar density plot. This CMD was divided into 2500 square bins, where we counted the number of stars and then normalized to the total number of

[1] http://www.cosmos.esa.int/web/gaia/science-performance

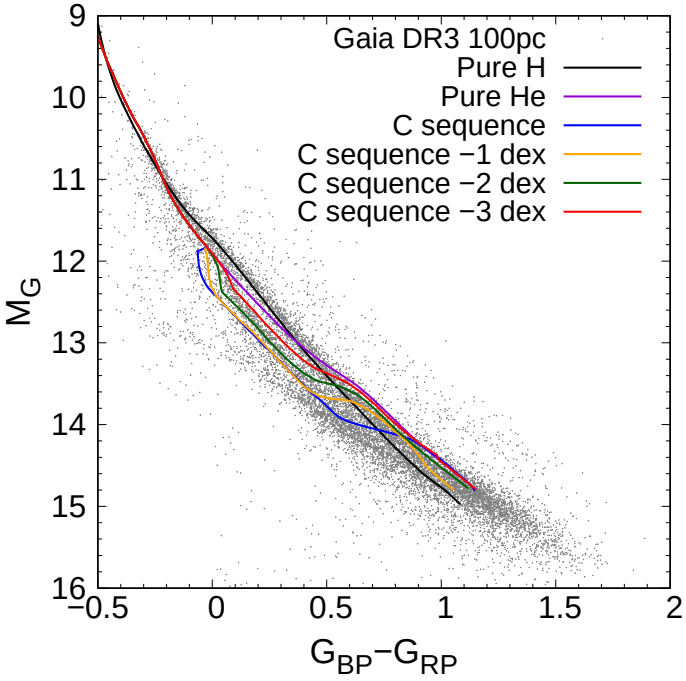

Fig. 3. Evolutionary tracks of a 0.58 $M_\odot$ white dwarf for different atmospheric compositions on the *Gaia* DR3 CMD, together with the observed 100 pc sample (gray dots). Evolutionary models considering pure H and pure He envelopes are displayed as black and purple lines, respectively. Models with a He atmosphere containing traces of C, and considering the C sequence, and the C sequence −1 dex, −2 dex, and −3 dex are shown using blue, orange, green, and red lines, respectively.

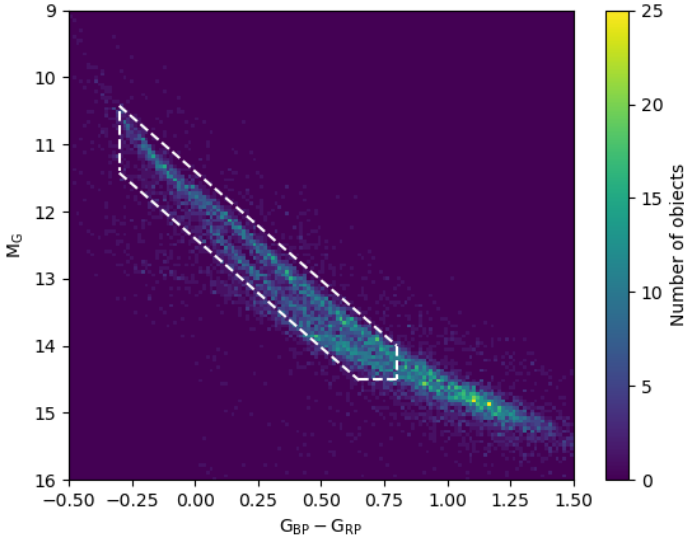

Fig. 4. Stellar density (Hess) diagram for the 100 pc thin-disk white dwarf sample in *Gaia* DR3. The white dashed lines delimit the region in which we perform the statistical analysis.

observed objects to perform a χ^2 statistical test (Mighell 1999). Each bin has a width of 0.04 mag in $G_{BP} - G_{RP}$, and a height of 0.14 mag in M_G. To avoid contamination from white dwarfs on the Q branch and faint white dwarfs, and to only take into account the objects on the bifurcation, we performed the χ^2 statistical test exclusively on the region delimited by the dashed white lines. By electing this region, we also avoid uncertainties

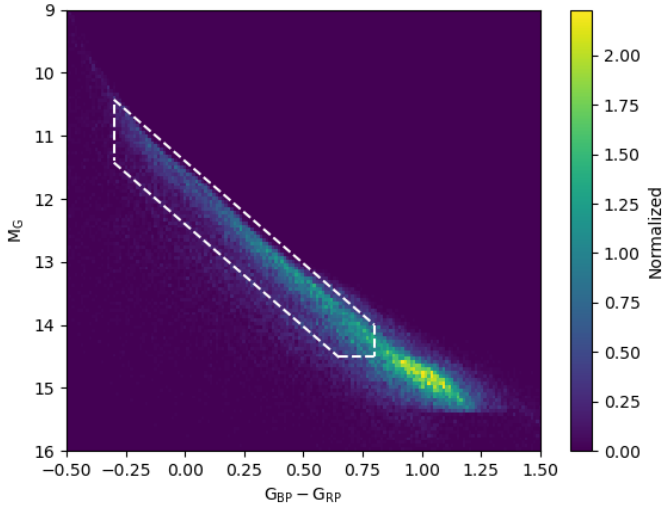

Fig. 5. Normalized Hess diagram for a synthetic 100 pc thin-disk white dwarf population considering 80% DA, 20% nonDA, pure-He composition for all nonDA white dwarfs, and the IFMR of Catalán et al. (2008).

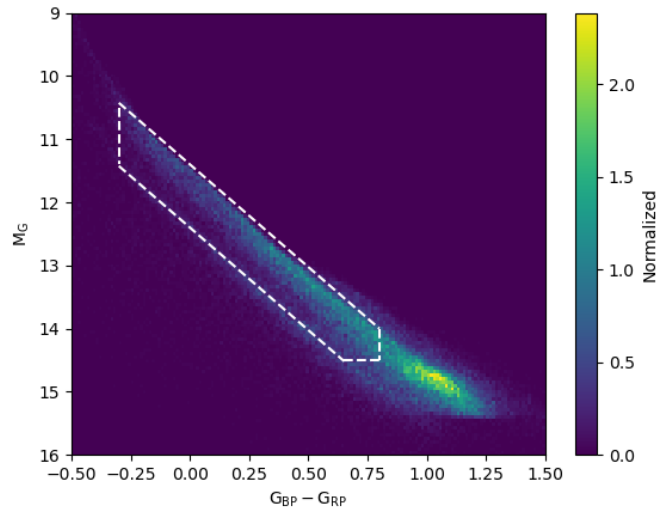

Fig. 6. Same as Fig. 5, but considering the IFMR of El-Badry et al. (2018).

arising from the star formation rate and the age assumed for the population.

We compared the observed sample with a total of 22 synthetic white dwarf populations varying the proportions of DA and nonDA white dwarfs, the C enrichment prescription for nonDA white dwarfs, and the IFMR. The quantities assumed for our synthetic populations are summarized in Table 1, together with the χ^2 value of the comparison with the observed sample.

In general lines, we find a better agreement when we include proportions of 80% DA and 20% nonDA, although populations with 75% DA, 25% nonDA and 70% DA, 30% nonDA white dwarfs also show a good agreement. Additionally, the IFMR of Catalán et al. (2008) yields a better reproduction of the bifurcation than the one by El-Badry et al. (2018), even when only DA white dwarfs are considered. A simple synthetic population considering 80% DA, 20% nonDA, a pure He composition for all nonDA white dwarfs, and an IFMR of Catalán et al. (2008) is shown in Fig. 5. We note that this synthetic population does not reproduce the *Gaia* bifurcation and has a relatively high value of

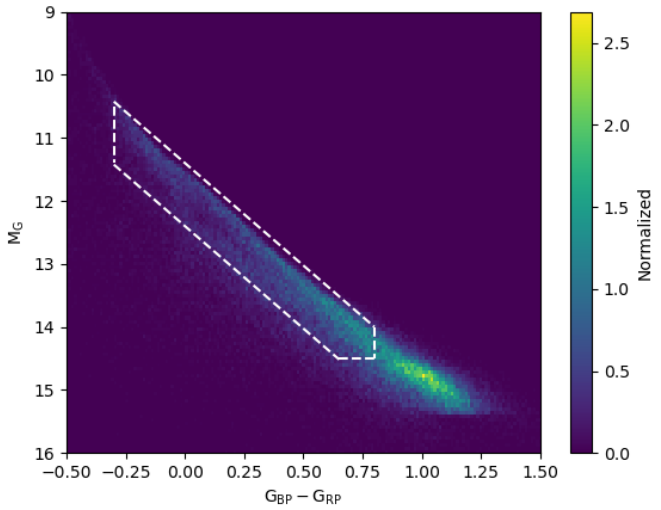

Fig. 7. Normalized Hess diagram for a synthetic 100 pc thin-disk white dwarf population considering 80% DA, 20% nonDA, an IFMR of Catalán et al. (2008), pure-He composition for all nonDA white dwarfs with $T_{\rm eff} > 12\,000$ K, and a random C-enrichment prescription (C random [0:2]) for all nonDA white dwarfs with $T_{\rm eff} < 12\,000$ K.

$\chi^2 = 3.816$. A similar synthetic population model – with the only difference being that it considers the IFMR of El-Badry et al. (2018) – is shown in Fig. 6. Using this IFMR produces many more white dwarfs with masses $\sim$0.8 $M_\odot$, but does not reproduce the *Gaia* bifurcation, its χ^2 value being as high as 7.863. On the contrary, considering the PG1159-DO-DB-DQ spectral evolution in all nonDA yields a much better agreement with the observations. In particular, we find the maximum agreement, that is, the lowest χ^2 value, when we consider a C enrichment that follows the C sequence ($\chi^2 = 2.972$). Figure 7 shows a synthetic population model that considers 80% DA, 20% nonDA, an IFMR of Catalán et al. (2008), a pure He composition for all nonDA white dwarfs with $T_{\rm eff} > 12\,000$ K, and a random C-enrichment prescription in the range [0:2] for all nonDA white dwarfs with $T_{\rm eff} < 12\,000$ K. We note a slight bifurcation in this figure caused by the C enrichment and resembling the *Gaia* bifurcation. The comparison of this synthetic population model with the observations gives $\chi^2 = 3.042$, which is slightly higher than the value for the best-fit population ($\chi^2 = 2.972$). Nevertheless, this synthetic population model is more realistic as it takes into account the fact that not all He-dominated white dwarfs can follow the C sequence. If all white dwarfs with He-dominated atmospheres were to follow the C sequence, there would be an enormous number of DQ white dwarfs observed, which is not the case. Synthetic population models that consist of 80% DA and 20% nonDA white dwarfs, following an IFMR of Catalán et al. (2008), and including C enrichment as the C sequence −1 dex or as C random [0:3] also provide a good fit, with χ^2 values of 3.191 and 3.147, respectively. Therefore, we conclude that, in general terms, we find much better agreement with the observations for synthetic population models that consider that nonDA white dwarfs follow a C enrichment than for synthetic population models that consider that all nonDA white dwarfs have a pure He envelope.

3.3. The mass distribution

On the basis of the spectral classification of Jiménez-Esteban et al. (2023), we determined the masses of 11 455 DA and 2295 nonDA white dwarfs within 100 pc. For each white dwarf with G and $G_{\rm BP}-G_{\rm RP}$, we made a linear interpolation in our evolutionary models to obtain its mass and effective temperature. In order to avoid extrapolation uncertainties, we excluded all DA WDs with masses lower than 0.239 $M_\odot$ and all nonDA WDs with masses lower than 0.51 $M_\odot$. For DA white dwarfs, we employed pure-H atmosphere models, whereas for nonDA white dwarfs we determined two different masses, varying the atmosphere model. In the first estimation, we considered that all nonDA white dwarfs have a pure He atmosphere and in the second one, we considered a pure He atmosphere if $T_{\rm eff} > 12\,000$ K and a C enrichment following the C sequence −1 dex if $T_{\rm eff} < 12\,000$ K.

The mass distributions obtained are shown in Fig. 8. The black histograms in the both panels show the mass distributions of DA white dwarfs. They exhibit a clear peak at $\sim$0.57 $M_\odot$, consistent with previous studies. We find a slight excess of DA white dwarfs with masses $\sim$0.8 $M_\odot$ as suggested by El-Badry et al. (2018), Kilic et al. (2018), but we also find a flattening in the DA mass distribution around 0.75 $M_\odot$, consistent with Kilic et al. (2020). Finally, we do not find a distinctive high-mass excess near 1.1 $M_\odot$ but rather some inkling near to this mass, as found by Rebassa-Mansergas et al. (2015), Hollands et al. (2018).

The mass distributions of nonDA white dwarfs are shown as purple and orange histograms in the left and right panels of Fig. 8, respectively. In the left panel, we employ pure He atmosphere models for all nonDA white dwarfs, whereas in the right panel, we consider the C enrichment commencing at $T_{\rm eff} = 12\,000$ K and following the C sequence −1 dex for all nonDA white dwarfs (i.e., stealth DQ white dwarfs are considered). The differences arising from the adoption of these treatments can be seen when comparing the purple and orange histograms in this figure. While considering a stealth C enrichment in the atmosphere (orange histogram) leads to a mass distribution more similar to the one for DA white dwarfs, considering a pure He atmosphere (purple histogram) leads to an excess of massive nonDA white dwarfs. Indeed, a surprising massive population of nonDA white dwarfs is obtained when pure He atmosphere models are considered. Such a massive population is not consistent with an isolated evolutionary channel for the formation of nonDA white dwarfs. The total mass distributions (DA + nonDA histograms) are shown as blue histograms in both panels. It is clear that considering a pure He envelope leads to an excess of massive ($\sim$0.75 $M_\odot$) white dwarfs caused by nonDA white dwarfs.

4. Summary and conclusions

Precise observations by the *Gaia* space mission have revealed a bifurcation of the CMD of the white dwarf population into two branches. The main goal of this paper is to provide an explanation for the B branch by investigating the effect of C contamination in the envelopes of He-rich white dwarfs.

There is significant evidence that C contamination occurs on cool He-rich white dwarfs as a result of convective dredge-up in the so-called PG1159-DO-DB-DQ spectral evolutionary channel. Theoretical models of He-dominated white dwarfs predict that an outer convective zone penetrates into C rich layers, leading to C dredge-up and the consequent growth of the surface C abundance. After the convective zone reaches its maximum depth, the partial recombination of C below the convective zone makes C sink back into the interior, leading to a slow and constant decrease in the surface C abundance. Although the models can predict the general behavior of C enrichment, they cannot predict the exact amount of C dredged-up, as this

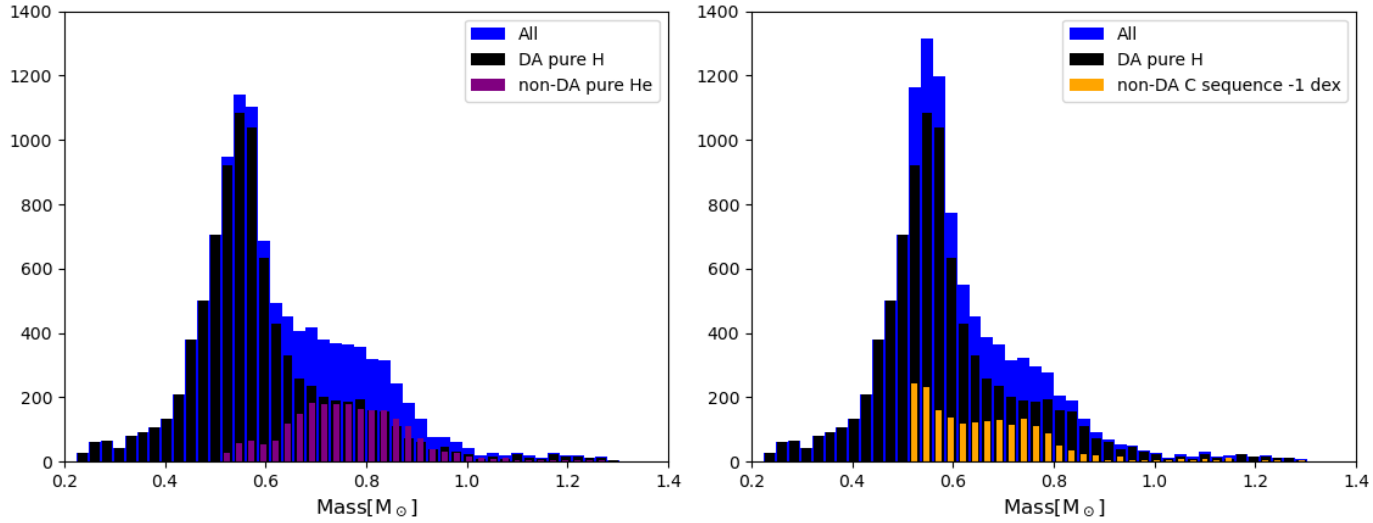

Fig. 8. Mass distributions of the 100 pc white dwarf population spectrally classified into DA and nonDA by Jiménez-Esteban et al. (2023). Left panel: we employed a pure H atmosphere model for all DA white dwarfs and a pure He atmosphere model for all nonDA white dwarfs. The black, purple and blue histograms are the mass distributions of DA, nonDA, and all white dwarfs, respectively. Right panel: same as left panel, but considering a C enrichment following the C sequence −1 dex for all nonDA white dwarfs. The orange histogram shows the mass distribution of these nonDA white dwarfs.

depends on the initial conditions and physical inputs considered. Relying on precise He-rich evolutionary models, we simulated the C enrichment under different prescriptions. We considered that all nonDA white dwarfs have a pure He atmosphere if their effective temperature is >12 000 K, and a He atmosphere with C traces if their effective temperature is <12 000 K. The first C contamination recipe consists in applying a least-squares fit to the C-to-He abundance ratio in terms of the effective temperature, observed in cold ($T_{\rm eff}$ < 10 000 K) DQ white dwarfs. For 12 000 K > $T_{\rm eff}$ > 10 000 K, we reflected this linear fit (see Sect. 2.2 for details). We call this type of C contamination the "C sequence". Three similar prescriptions for C contamination have also been considered, that is, by shifting the surface [C/He] abundance from the C sequence by −1 dex, −2 dex, and −3 dex. It is important to note that white dwarfs that follow the C-sequence enrichment have detectable traces of C in their optical spectra, but white dwarfs that follow the C-sequence enrichment −1 dex, −2 dex, and −3 dex do not. Therefore, we call these latter stars stealth DQ white dwarfs.

We find that the presence of trace C in the atmosphere of He-rich white dwarfs has an important effect on the continuum spectrum of these stars, enhancing the absorption in red wavelengths and thus creating the *Gaia* bifurcation. Indeed, the B branch of the *Gaia* bifurcation is consistent with a ∼0.6 $M_{\odot}$ stealth DQ evolutionary track. This shift is primarily caused by the He^- free-free absorption. The partial ionization of trace C leads to a substantial increase in the free electron density, leading to a higher number of He^- ions, which in turn amplifies the He^- free-free opacity. Therefore, even though stealth DQ white dwarfs do not show C lines or C molecular bands in their optical spectra, their continuum emission differs from the one expected for a pure He atmosphere. However, stealth DQ white dwarfs should have strong C signatures in their UV spectra, which would confirm the presence of trace C in their atmospheres.

We performed a population synthesis analysis of the white dwarfs on the *Gaia* bifurcation within 100 pc. We generated synthetic population models varying the IFMR, the proportions of DA and nonDA white dwarfs, and the nonDA atmospheric composition. We find the maximum agreement with the observations when nonDA models that take into account the C enrichment are considered in the synthetic population models. NonDA models with a pure He atmosphere fail to reproduce the B branch, even when the flatter IFMR of El-Badry et al. (2018) is considered. Among the different C enrichment prescriptions, we do not find significantly better agreement for any prescription in particular. The best χ^2 value is found when nonDA white dwarfs follow the C sequence parametrization, but the C sequence −1 dex parametrization also yields good agreement. Furthermore, the populations that consider that each white dwarf can randomly follow a different C-enrichment parametrization also show good agreement with the observations. We wish to remark that a synthetic population model in which all nonDA white dwarfs follow the C sequence enrichment is not realistic, as it is characterized by a large number of DQ white dwarfs, which are not detected in observed samples.

Finally, on the basis of the spectral classification of Jiménez-Esteban et al. (2023), we determined the white dwarf mass distributions of DA and nonDA white dwarfs within 100 pc. With G and $G_{\rm BP} - G_{\rm RP}$ for each individual white dwarf, we interpolated in our white dwarf evolutionary models to obtain its mass. For DA white dwarfs, we obtain a peak at ∼0.6 $M_{\odot}$ and a flattening around ∼0.8 $M_{\odot}$, in agreement with other mass distributions in the literature. For nonDA white dwarfs, we obtain two markedly different mass distributions, depending on whether we consider a pure He atmosphere or a He atmosphere with traces of C. On the one hand, if a pure He atmosphere is employed, the mass distribution exhibits a wide peak at ∼0.8 $M_{\odot}$, which is not consistent with the DA mass distribution or with the standard evolutionary channel for the formation of nonDA white dwarfs (i.e., late thermal pulses). On the other hand, when a mixed He/C atmosphere with "invisible" C traces is employed, we re-obtain the typical peak at ∼0.6 $M_{\odot}$.

In general, we find that the stealth DQ white dwarfs are much better at reproducing bifurcation in the *Gaia* CMD, as well as the mass distribution for nonDA white dwarfs, than pure He white dwarfs. Therefore, we propose that many of the spectrally classified DC white dwarfs in the B branch of the *Gaia* bifurcation could be stealth DQ white dwarfs with invisible trace C in their

optical spectra. Furthermore, Koester et al. (2020) estimated a He mass fraction in the envelope of cold DQs that is nearly one order of magnitude lower than that predicted by stellar evolutionary models. Therefore, it is likely that stealth DQ white dwarfs originate from white dwarfs with canonical He envelopes, which are consistent with the standard progenitor evolution. The trace C in some of these stars could potentially be detected in UV spectra. As only a few DC white dwarfs have been followed up with UV spectra, we encourage observational efforts in detecting C features on the UV spectra of white dwarfs on the B branch of the *Gaia* bifurcation.

Acknowledgements. The authors acknowledge the expert referee S. O. Kepler. MC acknowledges grant RYC2021-032721-I, funded by MCIN/AEI/10.13039/501100011033 and by the European Union NextGenerationEU/PRTR. MAH is supported by grant ST/V000853/1 from the Science and Technology Facilities Council (STFC). RR acknowledges support from Grant RYC2021-030837-I funded by MCIN/AEI/ 10.13039/501100011033 and by "European Union NextGenerationEU/PRTR". This work was partially supported by the AGAUR/Generalitat de Catalunya grant SGR-386/2021 and by the Spanish MINECO grant PID2020-117252GB-I00. This research made use of NASA Astrophysics Data System. This work made use of data from the European Space Agency (ESA) mission *Gaia* (https://www.cosmos.esa.int/gaia), processed by the *Gaia* Data Processing and Analysis Consortium (DPAC, https://www.cosmos.esa.int/web/gaia/dpac/consortium). Funding for the DPAC has been provided by national institutions, in particular the institutions participating in the *Gaia* Multilateral Agreement.

References

Althaus, L. G., Serenelli, A. M., Panei, J. A., et al. 2005, A&A, 435, 631
Althaus, L. G., Panei, J. A., Miller Bertolami, M. M., et al. 2009, ApJ, 704, 1605
Althaus, L. G., Córsico, A. H., Isern, J., & García-Berro, E. 2010, A&A Rev., 18, 471
Althaus, L. G., Camisassa, M. E., Miller Bertolami, M. M., Córsico, A. H., & García-Berro, E. 2015, A&A, 576, A9
Bauer, E. B., Schwab, J., Bildsten, L., & Cheng, S. 2020, ApJ, 902, 93
Bédard, A., Bergeron, P., Brassard, P., & Fontaine, G. 2020, ApJ, 901, 93
Bédard, A., Bergeron, P., & Brassard, P. 2022, ApJ, 930, 8
Bédard, A., Bergeron, P., & Brassard, P. 2023, ApJ, 946, 24
Bergeron, P., Dufour, P., Fontaine, G., et al. 2019, ApJ, 876, 67
Blouin, S., Dufour, P., Thibeault, C., & Allard, N. F. 2019, ApJ, 878, 63
Blouin, S., Daligault, J., & Saumon, D. 2021, ApJ, 911, L5
Camacho, J., Torres, S., García-Berro, E., et al. 2014, A&A, 566, A86
Camisassa, M. E., Althaus, L. G., Córsico, A. H., et al. 2016, ApJ, 823, 158
Camisassa, M. E., Althaus, L. G., Rohrmann, R. D., et al. 2017, ApJ, 839, 11
Camisassa, M. E., Althaus, L. G., Córsico, A. H., et al. 2019, A&A, 625, A87
Camisassa, M. E., Althaus, L. G., Torres, S., et al. 2021, A&A, 649, L7
Camisassa, M. E., Althaus, L. G., Koester, D., et al. 2022, MNRAS, 511, 5198
Canals, P., Torres, S., & Soker, N. 2018, MNRAS, 480, 4519
Caplan, M. E., Freeman, I. F., Horowitz, C. J., Cumming, A., & Bellinger, E. P. 2021, ApJ, 919, L12
Catalán, S., Isern, J., García-Berro, E., & Ribas, I. 2008, MNRAS, 387, 1693
Chambers, K. C., Magnier, E. A., Metcalfe, N., et al. 2016, ArXiv e-prints [arXiv:1612.05560]
Cheng, S., Cummings, J. D., & Ménard, B. 2019, ApJ, 886, 100
Cojocaru, R., Rebassa-Mansergas, A., Torres, S., & García-Berro, E. 2017, MNRAS, 470, 1442
Córsico, A. H., Althaus, L. G., Miller Bertolami, M. M., & Kepler, S. O. 2019, A&A Rev., 27, 7
Dufour, P., Bergeron, P., & Fontaine, G. 2005, ApJ, 627, 404
Dunlap, B. H., & Clemens, J. C. 2015, in 19th European Workshop on White Dwarfs, eds. P. Dufour, P. Bergeron, & G. Fontaine, ASP Conf. Ser., 493, 547
El-Badry, K., Rix, H.-W., & Weisz, D. R. 2018, ApJ, 860, L17
Fleury, L., Caiazzo, I., & Heyl, J. 2022, MNRAS, 511, 5984
Fontaine, G., & Brassard, P. 2008, PASP, 120, 1043
Gaia Collaboration (Babusiaux, C., et al.) 2018, A&A, 616, A10
Gaia Collaboration (Brown, A. G. A., et al.) 2021, A&A, 649, A1
García-Berro, E., & Oswalt, T. D. 2016, New Astron. Rev., 72, 1
García-Berro, E., Torres, S., Isern, J., & Burkert, A. 1999, MNRAS, 302, 173
García-Berro, E., Torres, S., Althaus, L. G., et al. 2010, Nature, 465, 194
Gentile Fusillo, N. P., Tremblay, P. E., Cukanovaite, E., et al. 2021, MNRAS, 508, 3877
Hidalgo, S., Pietrinferni, A., Cassisi, S., et al. 2018, ApJ, 856, 125
Hollands, M. A., Tremblay, P. E., Gänsicke, B. T., Gentile-Fusillo, N. P., & Toonen, S. 2018, MNRAS, 480, 3942
Isern, J., Torres, S., & Rebassa-Mansergas, A. 2022, Front. Astron. Space Sci., 9, 6
Jiménez-Esteban, F. M., Torres, S., Rebassa-Mansergas, A., et al. 2018, MNRAS, 480, 4505
Jiménez-Esteban, F. M., Torres, S., Rebassa-Mansergas, A., et al. 2023, MNRAS, 518, 5106
Kawka, A., Ferrario, L., & Vennes, S. 2023, MNRAS, 520, 6299
Kepler, S. O., Koester, D., Pelisoli, I., Romero, A. D., & Ourique, G. 2021, MNRAS, 507, 4646
Kilic, M., Hambly, N. C., Bergeron, P., Genest-Beaulieu, C., & Rowell, N. 2018, MNRAS, 479, L113
Kilic, M., Bergeron, P., Kosakowski, A., et al. 2020, ApJ, 898, 84
Koester, D. 2010, Mem. Soc. Astron. Ital., 81, 921
Koester, D., & Kepler, S. O. 2019, A&A, 628, A102
Koester, D., Weidemann, V., & Zeidler, E. M. 1982, A&A, 116, 147
Koester, D., Kepler, S. O., & Irwin, A. W. 2020, A&A, 635, A103
Mighell, K. J. 1999, ApJ, 518, 380
Miller Bertolami, M. M. 2016, A&A, 588, A25
Miller Bertolami, M. M., & Althaus, L. G. 2006, A&A, 454, 845
Ourique, G., Kepler, S. O., Romero, A. D., Klippel, T. S., & Koester, D. 2020, MNRAS, 492, 5003
Pelletier, C., Fontaine, G., Wesemael, F., Michaud, G., & Wegner, G. 1986, ApJ, 307, 242
Raddi, R., Torres, S., Rebassa-Mansergas, A., et al. 2022, A&A, 658, A22
Rebassa-Mansergas, A., Rybicka, M., Liu, X. W., Han, Z., & García-Berro, E. 2015, MNRAS, 452, 1637
Rebassa-Mansergas, A., Maldonado, J., Raddi, R., et al. 2021, MNRAS, 505, 3165
Renedo, I., Althaus, L. G., Miller Bertolami, M. M., et al. 2010, ApJ, 717, 183
Ricker, G. R., Winn, J. N., Vanderspek, R., et al. 2015, J. Astron. Telesc. Instrum. Syst., 1, 014003
Salaris, M., Cassisi, S., Pietrinferni, A., & Hidalgo, S. 2022, MNRAS, 509, 5197
Serenelli, A., Rohrmann, R. D., & Fukugita, M. 2019, A&A, 623, A177
Steinmetz, M., Guiglion, G., McMillan, P. J., et al. 2020a, AJ, 160, 83
Steinmetz, M., Matijevič, G., Enke, H., et al. 2020b, AJ, 160, 82
Torres, S., & García-Berro, E. 2016, A&A, 588, A35
Torres, S., García-Berro, E., Isern, J., & Figueras, F. 2005, MNRAS, 360, 1381
Torres, S., García-Berro, E., Althaus, L. G., & Camisassa, M. E. 2015, A&A, 581, A90
Torres, S., García-Berro, E., Cojocaru, R., & Calamida, A. 2018, MNRAS
Torres, S., Cantero, C., Rebassa-Mansergas, A., et al. 2019, MNRAS, 485, 5573
Torres, S., Rebassa-Mansergas, A., Camisassa, M. E., & Raddi, R. 2021, MNRAS, 502, 1753
Torres, S., Canals, P., Jiménez-Esteban, F. M., Rebassa-Mansergas, A., & Solano, E. 2022, MNRAS, 511, 5462
Tremblay, P.-E., Fontaine, G., Fusillo, N. P. G., et al. 2019, Nature, 565, 202
Winget, D. E., & Kepler, S. O. 2008, ARA&A, 46, 157
York, D. G., Adelman, J., Anderson, J. E., Jr, et al. 2000, AJ, 120, 1579